Tunneling Properties of the Charge Carriers through Sub-2-nm-Thick Oxide in Ge/*a*-GeO_2/Ge Structures Using the First-Principles Scattering-State Method

Eunjung Ko,[1] Kai Liu,[1,2] Cheol Seong Hwang,[2] Hyoung Joon Choi,[3] and Jung-Hae Choi[1,*]

[1] *Center for Electronic Materials, Korea Institute of Science and Technology, Seoul 02792, Korea*

[2] *Department of Materials Science and Engineering and Inter-University Semiconductor Research Center, Seoul National University, Seoul 08826, Korea*

[3] *Department of Physics and IPAP, Yonsei University, Seoul 03722, Korea*

(Received 20 August 2018; revised manuscript received 20 December 2018; published 7 March 2019)

The quantum-mechanical tunneling passing through the sub-2-nm-thick oxide in Ge/*a*-GeO_2/Ge structures is presented, using the first-principles scattering-state method, where *a* stands for the amorphous phase. The suboxide interface layer (IL) between Ge and the dioxide region (DOX) does not play a critical role in blocking tunneling due to the presence of Ge—Ge bonds in it. The thickness of DOX, where all the Ge has four Ge—O bonds, is the effective tunneling-blocking thickness and the thickness for the thinnest usable *a*-GeO_2 is approximately 0.85 nm. The width and magnitude of the band offset differently affect the tunneling in the sub-2-nm-thick oxide. The valence-band offset is larger and thicker than the conduction-band offset for all the structures, resulting in the smaller tunneling current of the holes than of the electrons. It is also found that the effect of the hydrogen passivation at the IL on tunneling is not evident in semiconductor/*a*-oxide. The crystallographic orientation of Ge has no distinct effect on the band-gap alignment and the tunneling current in Ge/*a*-GeO_2/Ge structures, consistent with the experimental results about the effect of the Ge orientation on the interface properties.

DOI: 10.1103/PhysRevApplied.11.034016

I. INTRODUCTION

Since the emergence of the downscaling of the Si-based metal oxide semiconductor (MOS) devices in the early 1970s, the quantum-mechanical tunneling current passing through the oxide has been one of the crucial limiting factors in device downscaling. The limitation of the downscaling of Si devices has stirred up the search for the next-generation channel materials with high device performance. Ge has received attention again of late as one of the promising next-generation channel materials, owing to its excellent electron and hole mobilities compared to Si as well as the high device performance by the use of a passivation layer between the Ge channel and high-*k* materials to relieve the poor electrical characteristics of GeO and GeO_2 at the Ge/high-*k* oxide interface [1]. Moreover, from the industrial viewpoint, Ge is the most possible next-generation channel material because its atomic structure is similar to that of Si, enabling the continuous usage of the present Si-based industrial equipment [1].

For the successful usage of Ge MOS devices as frequently as Si MOS devices, the tunneling leakage currents induced from the downscaling of Ge devices should be less than or at least comparable to those induced from the downscaling of Si devices. Experimentally, considerable work on the gate leakage currents in Ge devices with various high-*k* materials has been performed [2–4]. The properties of the tunneling passing through the GeO_2 in Ge/GeO_2 structures, however, have not been extensively examined.

In the downscaled MOS devices, the oxides are approximately sub-2-nm thick, and as such, the direct tunneling current is very important; therefore, the interfacial atomic structures have crucial effects on the tunneling properties. For Si MOS structures such as Si/SiO_2/Si structures, the first-principles calculations of the tunneling properties showed the effects of three-dimensional (3D) atomic structures on the tunneling current through the ultrathin SiO_2 layers [5–8]. No theoretical study has been performed to date on the tunneling properties in Ge/GeO_2 or any Ge-based MOS structure. The calculation works on Ge/GeO_2, Ge/high-*k*, and Ge/passivation layer/high-*k* structures to date have been limited to interface properties and electronic properties [9–12].

In the recently developed 3D-structure transistors such as the trigate transistor and the fin field-effect transistor developed for smaller microprocessors and memory cells, the gate oxides are faced with different Ge substrate orientations, making it valuable to examine the gate leakage current densities along different Ge orientations. While it

*choijh@kist.re.kr

is known that the Ge(111) and Ge(110) surfaces can provide the highest electron and hole mobilities, respectively [13], a recent experimental study of Ge/GeO_2 interfaces showed that the conduction barrier height evaluated from the gate current conduction mechanism is almost the same for the Ge(100), Ge(110), and Ge(111) orientations [14]. This implies a very weak dependence of the gate leakage currents on the Ge orientation, but no theoretical work has been done to confirm this.

In this paper, we present the atomic-structure-dependent tunneling properties passing through sub-2-nm-thick a-GeO_2 in Ge/a-GeO_2/Ge structures with different oxide thicknesses, interfacial structures, and Ge orientations obtained by the first-principles scattering-state method [15]. This work shows that only the stoichiometric dioxide region (DOX) excluding the IL is effective for blocking the leakage current and suggests a critical oxide thickness of approximately 0.85 nm for the thinnest usable a-GeO_2. A specific relation between band offsets and tunneling spectra in the sub-2-nm-thick oxide is addressed. It is shown that the valence-band offset (VBO) is larger in magnitude and wider in space than the conduction-band offset (CBO), which results in the smaller tunneling current of the holes than of the electrons. It is also found that the hydrogen passivation at the semiconductor/a-oxide interface is not very effective in reducing the tunneling current by removing the dangling bonds. Lastly, it is shown that the tunneling current is hardly dependent on the crystallographic orientation of Ge in Ge/a-GeO_2/Ge structures.

II. RESULTS AND DISCUSSION

To determine the effects of sub-2-nm-thick a-GeO_2 oxides on the tunneling properties of the charge carriers of Ge, Ge/a-GeO_2/Ge heterostructures, so called GA structures, are generated as the preparation procedure explained in the Appendix and the Supplemental Material [16] in detail. For these heterostructures, the following are investigated: (1) the detailed atomic structures, (2) the electronic structures such as the band gap and the band offset, and (3) the tunneling properties of the electrons and holes through the thin oxides. The changes in the oxide thickness and the suboxide distribution at the interface are considered, along with the presence of dangling bonds or their hydrogen passivation at the interface. GA structures with three different Ge orientations [(100), (110), and (111)] are also investigated.

For the atomic and electronic structures, first-principles electronic structure calculations are performed based on the density-functional theory (DFT). Table I summarizes the calculated lattice constant of bulk Ge and the mass density of bulk a-GeO_2 in comparison with the experimental value. The calculated lattice constant of Ge is almost the same as the experimental value. The a-GeO_2 structures are generated by first-principles molecular dynamics [17,18], reproducing the experimental mass density of 3.6 g cm^{-3} [19].

TABLE I. Lattice constant (a) of the Ge bulk phase calculated by LDA and mass density (d) of the a-GeO_2 bulk phases that are used, with band gaps (E_g) of the bulk phases of Ge and a-GeO_2 calculated using the LDA and LDA + U methods. All the data are compared with the available experimental values (Expt.): $U = 0.73$ eV and $J = -0.44$ eV for (1) LDA + U and $U = 3.00$ eV and $J = 0.00$ eV for (2) LDA + U.

		Ge	a-GeO_2
a (nm)	LDA	0.564	
	Expt.	0.566	
d (g cm^{-3})	LDA		3.6
	Expt.		3.6 [19]
E_g (eV)	LDA	0.2	4.6
	(1) LDA+U	0.4	4.6
	(2) LDA+U	0.7	4.6
	Expt.	0.66	5.6 [20]

For the atomic structure, the local density approximation (LDA) is used. Then, the LDA + U method is used to investigate the electronic structures and the tunneling properties of the Ge/a-GeO_2/Ge structures within the practically available computational time as well as to correct the band gap of the whole system. The LDA + U method describes the electron correlation and is effective only when it is applied on the occupied orbitals. In the LDA + U method for bulk Ge, two different parameter sets (on-site Coulomb interaction U and Hund's coupling J) are used for the 4p orbitals of Ge, which mainly contributes the valence-band maximum (VBM). One set consists of $U = 0.73$ eV and $J = -0.44$ eV, which is obtained by the constrained LDA method [21,22], resulting in the band-gap increase of Ge from 0.2 eV (without using $+U$) to 0.4 eV. These U and J parameters are systemically computed in the aim of describing the effective interactions among correlated electrons within the LDA method. The other set consists of $U = 3.00$ eV and $J = 0.00$ eV, which is fitted to the experimental band gap of 0.7 eV. This $+U$ scheme on the 4p orbitals of Ge does not affect the band gap of bulk a-GeO_2, because the VBM of a-GeO_2 mainly consists of the 2p orbitals of O atoms, while the conduction-band minimum (CBM) of the bulk a-GeO_2 is mainly composed of the 4p orbitals of Ge. The LDA + U is not applied to the 2p orbitals of O atoms, because the band gap of a-GeO_2 slabs in the Ge/a-GeO_2/Ge structures is similar to that of the available experimental values as shown in Table III and further discussion in Fig. 2. Hereafter, the first parameter set of the LDA + U is mainly used. The effect of the increase in the band gap of Ge from 0.4 eV [set (1)] to 0.7 eV [set (2)] is discussed in Fig. 3.

Figure 1 shows a relaxed GA structure composed of a-GeO_2 placed between two Ge(100) slabs, where the

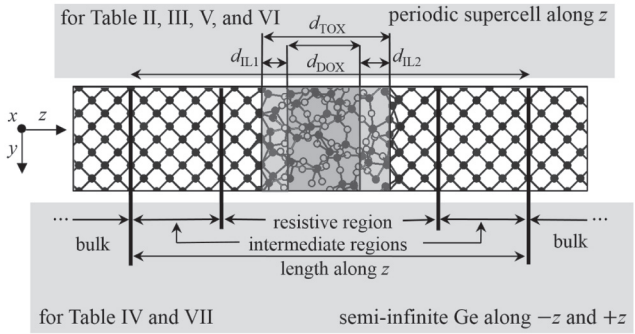

FIG. 1. Relaxed atomic structure for Ge/a-GeO_2/Ge (GA). The black circle is for Ge, while the white circle is for O. The interface layer (IL) and the dioxide region (DOX) are colored light gray and dark gray, respectively. The structure with dangling bonds at the IL (DB IL) is shown, and the corresponding H-passivated structure (HP IL) is omitted. In the upper part, the periodic cell along the z-axis is indicated for the calculations of the atomic and electronic structures. On the other hand, in the lower part, the resistive region, two intermediate regions, and bulk regions are defined for the transport calculations.

black and white circles indicate the Ge and O atoms, respectively. The total oxide region (TOX) is divided into the dioxide region (DOX) and the interface layer (IL), as shown in the upper part of the figure. DOX is defined as a region composed only of the Ge^{4+} state (four Ge—O bonds), indicated by the dark gray color. On the contrary, IL is defined as a region composed mostly of suboxide states of Ge, with some Ge^{4+} states, which is shaded light gray. The suboxide states are Ge^{1+}, Ge^{2+}, and Ge^{3+}, which have one, two, and three Ge—O bonds, respectively. In this work, two different interfacial structures are considered: IL with dangling bonds (DB IL) and IL passivated by H atoms (HP IL) (the figure with HP IL is not shown). The total thickness of the oxide, d_{TOX}, is the sum of the thickness of the DOX, d_{DOX}, and those of the two ILs, d_{IL1} and d_{IL2} ($d_{TOX} = d_{DOX} + d_{IL1} + d_{IL2}$). The thickness of IL, d_{IL}, for each structure is obtained from the average of d_{IL1} and d_{IL2} [$d_{IL} = (d_{IL1} + d_{IL2})/2$].

Four GA atomic models are investigated, labeled 1, 2, 3, and 4 as shown in Table II, when the orientation of Ge is (100). Table II shows the periodic supercell size along the z axis; the numbers of the Ge and O atoms in the periodic supercell; the cross-sectional area of heterostructure A; the oxide thicknesses of d_{TOX}, d_{DOX}, and d_{IL}; the numbers of Ge atoms in the suboxide states; and the numbers of defects and H atoms for each IL. The number of defects is calculated as [4−(number of Ge—O bonds)−(number of Ge—Ge bonds)]. For this, the maximum bond length is defined as 1.2×(sum of two atoms' covalent radii) and they are set as 0.293 nm for Ge—Ge and 0.234 nm for Ge—O, respectively. It should be pointed out that the number of defects in the DB IL is not the same as the number of passivating H atoms in the corresponding HP IL. At the ILs, the bond angles and bond lengths around the cations deviate from those of the regular tetrahedron due to the amorphous nature of the oxide. Therefore, only the effectively passivating H atoms are included in the HP IL by removing H atoms that produce gap states.

As shown in Table II, for all the structures, the d_{TOX} values range from 0.600 to 2.419 nm, and the d_{DOX} values range from 0 to 1.801 nm. The average d_{IL} value turns out to be 0.283 ± 0.027 nm for the GA structures. Note that in the sub-2-nm oxide thickness, the d_{IL} value for each GA structure is not negligible compared to the d_{TOX} and d_{DOX} values. For example, the average total IL thickness value ($d_{IL1} + d_{IL2}$) is about 0.584 nm, which is thicker than the unit-cell dimension of 0.564 nm in bulk Ge. Such a non-negligible d_{IL} value compared to the d_{TOX} and d_{DOX} values motivates us to carefully examine the electronic structures and the tunneling properties at the IL.

TABLE II. Relaxed atomic structures of Ge(100)/a-GeO_2/Ge(100) (GA1–GA4) with different oxide thicknesses.

Structure	GA1	GA2	GA3	GA4
Supercell along z axis (nm)	4.748	5.155	5.597	6.527
Number of Ge/O	263/18	276/40	288/64	320/128
A (nm^2)		1.129 × 1.129 ($2a_{Ge} \times 2a_{Ge}$)		
d_{TOX} (nm)	0.600	0.973	1.354	2.419
d_{DOX} (nm)	0.000	0.421	0.854	1.801
d_{IL} (nm)	0.300	0.276	0.250	0.309
$d_{IL,ave}$ (nm)		0.283 ± 0.027		
Number of suboxide states, defects, H atoms in ILs				
$Ge(Si)^{1+}$	11	10	10	5
$Ge(Si)^{2+}$	5	5	4	8
$Ge(Si)^{3+}$	3	3	5	3
$Ge(Si)^{4+}$	2	3	1	1
Defect(DB)	1	4	7	9
H(HP)	0	3	2	9

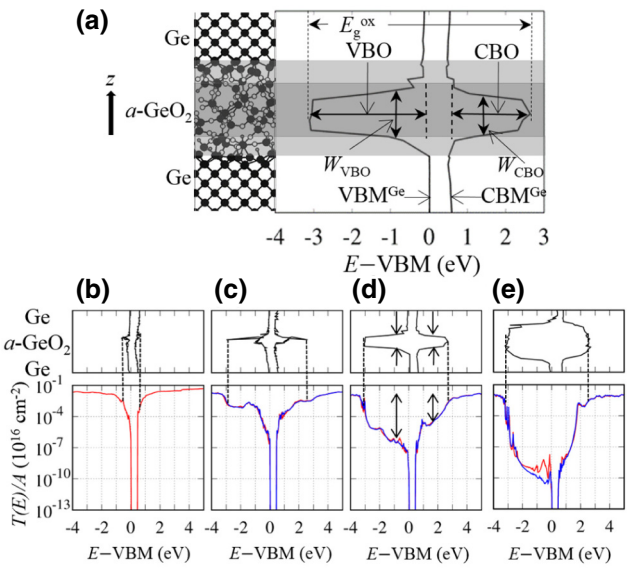

FIG. 2. (a) Atomic structure and band-gap alignment with respect to the IL and DOX in the GA3 structure with the HP IL. In the left panel, the black, white, and gray circles indicate the Ge, O, and H atoms, respectively. In the right panel, the band offsets (VBO and CBO), the widths of the band offsets (W_{VBO} and W_{CBO}), the oxide band gap (E_g^{ox}), the VBM of Ge ($\mathrm{VBM}^{\mathrm{Ge}}$), and the CBM of Ge ($\mathrm{CBM}^{\mathrm{Ge}}$) are indicated. The upper panel shows the band-gap alignment and the lower panels show the tunneling spectra per unit area $T(E)/A$ of (b)–(e) GA1, GA2, GA3, and GA4 structures. The band-gap alignments are obtained using the HP IL structures. In the lower panel, the red lines indicate the DB IL structures and the blue lines indicate the HP IL structures.

Figure 2(a) shows a representative example of the band-gap alignment along the z axis of the GA3 structure with the HP IL. For the over-2-nm-thick oxide, previous studies examined the effect of the magnitudes and widths of the band offsets on the tunneling properties, oversimplifying the atomic structures at the interface and neglecting d_{IL} due to $d_{\mathrm{IL}} \ll d_{\mathrm{TOX}}$, d_{DOX} [23]. In the sub-2-nm-thick oxide, however, the magnitudes and widths of the band offsets should be investigated more thoroughly because the portion of d_{IL} is not negligible compared with those of d_{TOX} and d_{DOX}. Furthermore, under such a circumstance, the band gap of the oxide evolves from a partially formed state to a fully formed state as the oxide thickness increases.

To examine the effects of the widths of the band offsets on the tunneling properties, the width of VBO (W_{VBO}) and the width of CBO (W_{CBO}) are defined. As can be seen in Fig. 2(a), the band offsets in the oxide region very near the VBM of the Ge region ($\mathrm{VBM}^{\mathrm{Ge}}$) and the CBM of the Ge region ($\mathrm{CBM}^{\mathrm{Ge}}$) show too-noisy data caused by the interface states. Therefore, the W_{VBO} and W_{CBO} are measured at 1.0 eV below $\mathrm{VBM}^{\mathrm{Ge}}$ and above $\mathrm{CBM}^{\mathrm{Ge}}$, respectively. The band offsets gradually increase from the IL to the DOX and they have the maximum values of the VBO and CBO within the DOX, as reported by the previous computational works on the $\mathrm{Si/SiO_2}$ interface [24]. This implies that only the DOX can be an effective potential barrier, not the TOX. In the sub-2-nm-thick oxide, such a gradual increase of the band offsets from the IL to the DOX becomes significant due to the ultrathin oxide and results in the thickest widths of the band offsets near $\mathrm{VBM}^{\mathrm{Ge}}$ and $\mathrm{CBM}^{\mathrm{Ge}}$. This result significantly influences the tunneling spectra and the tunneling current density, as shown in Figs. 2 and 3, respectively.

The upper panels of Figs. 2(b)–2(e) show the band-gap evolution for the GA structures with different oxide thicknesses. Table III summarizes their oxide band gap (E_g^{ox}), VBO, CBO, W_{VBO}, and W_{CBO} values calculated by the LDA + U method. The band-gap evolution is drawn using the atom-projected density of states [PDOS(z, E)] of the Ge atoms for the HP IL structures. The local VBM(z, E) and CBM(z, E) values are decided by neglecting the PDOS less than 0.03 states/eV so as to visualize the band-gap evolution; therefore, the average values for VBO and CBO in each structure are only estimated values. The E_g^{ox} is obtained as VBO + CBO + E_g^{Ge} (0.4 eV), as indicated by the black vertical dashed lines. When the a-$\mathrm{GeO_2}$ slab is too thin, the band gap partially forms such as the GA1 and GA2 structures. In the GA3 and GA4 structures, in contrast, the calculated E_g^{ox} values of the slab a-$\mathrm{GeO_2}$ are 5.90 and 5.87 eV, respectively. They are slightly larger than that of the bulk a-$\mathrm{GeO_2}$ of 4.6 eV but are comparable to the experimental bulk value of 5.6 eV. This result might be caused by the approximated PDOS estimation method in this study as well as the inherent effect of the thin slab. For Ge/a-$\mathrm{GeO_2}$ interfaces with 1–2-nm thick a-$\mathrm{GeO_2}$, experimental reports on the band gap of a-$\mathrm{GeO_2}$, CBO, and VBO are not available. For the Ge/a-$\mathrm{GeO_2}$ interfaces with $d_{\mathrm{GeO_2}} \geq 25$ nm [25], on the other hand, they are 5.76, 1.5, and 3.6 eV, respectively, and are expected to be similar to those of Ge/a-$\mathrm{GeO_2}$ interfaces with 1–2-nm thick a-$\mathrm{GeO_2}$. The calculated oxide band gap, CBO, and VBO for the GA4 structure ($d_{\mathrm{DOX}} = 1.801$ nm) are 5.87, 2.26, and 3.21 eV and they are quite in accordance with the experimental values. It is noted that the tendency of the lower CBO than VBO observed in the experiments is also shown in our theoretical band offsets of all the GA structures. It implies that the application of the LDA + U method only on the $4p$ orbitals of Ge atoms is appropriate for the purpose of correcting the band gap and the band offset of the whole Ge/a-$\mathrm{GeO_2}/\mathrm{Ge}$ structures.

It is important to point out that the effective oxide thickness for preventing the tunneling of the charge carriers is d_{DOX}, not d_{TOX}. This result is based on the fact that the band offsets gradually increase from the IL to the DOX and that the maximum VBO and CBO exist only inside the DOX, as shown in Fig. 2(a). The tunneling wave function effectively decays inside the DOX, not within the IL, where the charge carriers may tunnel through the Ge—Ge

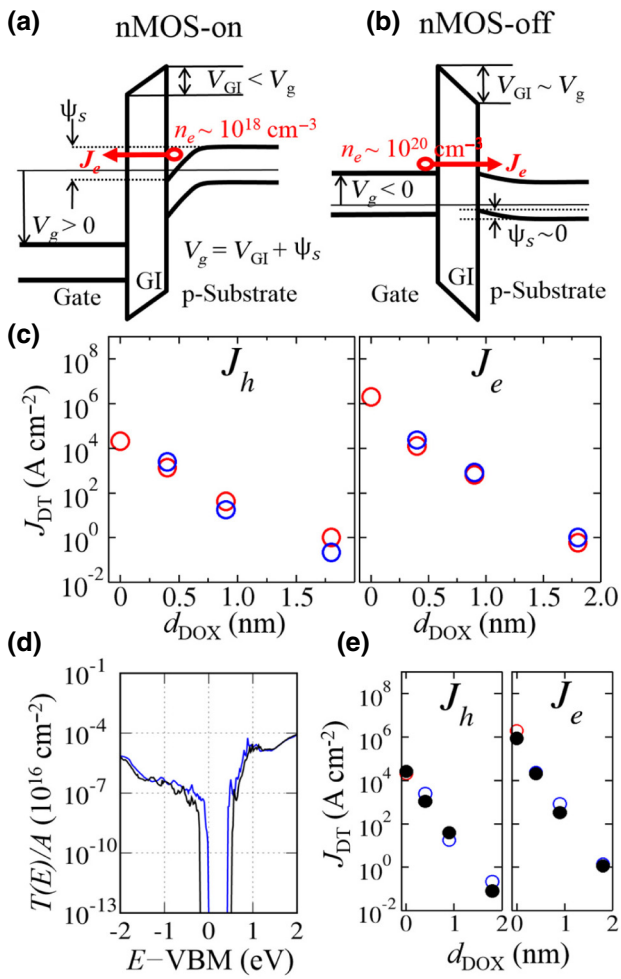

FIG. 3. Schematics of tunneling (a) under the (strong) inversion condition and (b) under the accumulation and reliability test in the Ge/a-GeO_2/Ge structure. V_g, V_{GI}, and ψ_s are the gate voltage, the voltage of the gate insulator, and the surface potential of Ge, respectively. (c) Direct tunneling current density J_{DT} as a function of d_{DOX} for Ge/a-GeO_2/Ge. In (c), the red symbols indicate the DB IL structures, while the blue symbols indicate the HP IL structures. In (c) and (e), the charge carrier concentrations are $n_{e,h} = 10^{18}$ cm^{-3}. Effects of the Ge band-gap correction from 0.4 eV (blue/red) to 0.7 eV (black) on (d) $T(E)/A$ and (e) J_{DT}. (d) is for the GA3 structure with the HP IL and (e) for the GA1 structure with the DB IL and the GA2, GA3, and GA4 structures with the HP IL. The GA1 structure does not have any available HP IL structure.

or Si—Si bonds. One drastic example of this is the GA1 structure shown in Fig. 2(b), where E_g^{ox} hardly forms due to the zero d_{DOX}, even though the d_{TOX} is 0.6 nm. In this case, the TOX consists only of an IL.

In Table III, the d_{DOX} of approximately 0.85 nm is suggested to be the critical thickness for GA structures. When the d_{DOX} is in the range of sub-0.85 nm, the E_g^{ox}, VBO, CBO, W_{VBO}, and W_{CBO} gradually increase as the d_{DOX} increases. On the contrary, when the d_{DOX} is in the range of more than 0.85 nm, only the W_{VBO} and W_{CBO} increase as the d_{DOX} increases with the fully formed E_g^{ox}, VBO, and CBO retained. For example, the E_g^{ox}, VBO, and CBO in the GA3 structure with a d_{DOX} of 0.854 nm are already fully formed; therefore, only the W_{VBO} and W_{CBO} increase in the GA4 structure with a thicker d_{DOX} of 1.801 nm. For the sub-1 nm oxide in Si/a-SiO_2/Si structures, on the other hand, a previous study [26] suggested that the minimum thickness at which the oxide blocks the tunneling would be 0.7 nm.

To investigate the tunneling properties of the charge carriers in GA structures, first-principles transport calculations are performed using the first-principles scattering-state method [15]. This method is one of the first-principles transport methodologies based on DFT, which considers detailed atomic structures and simulates both the linear and nonlinear electrical transport properties of a nanometer-scale system without assuming any periodic boundary condition along the current direction. As indicated in the lower part of Fig. 1, the atomic structure for the transport calculation is periodic in the x and y axes but is not periodic in the z axis, and a nanometer-thick oxide region is placed between the two bulk regions of Ge, which are semi-infinite in the $+z$ and $-z$ directions, respectively. In transport calculations, each heterostructure is regarded as composed of five regions for the theoretical description: a resistive region, two intermediate regions, and two semi-infinite bulk regions. Table IV shows the length along z, which is the sum of the z dimension of the resistive region and those of the two intermediate regions and the numbers of Ge and O atoms in these regions.

The lower panels of Figs. 2(b)–2(e) show the tunneling spectra per unit area, $T(E)/A$, where A is the cross-sectional area of the supercell and $T(E)$ are the average tunneling probabilities at the charge carrier energy E over all the tunneling channels n and the component $k_{||}$ of the wave vector parallel to the interface [i.e., $T(E) = (1/N_{k_{||}}) \sum_{n,k_{||}} T_n(E, k_{||})$]. Each tunneling probability is estimated by the scattering-state wave function $\psi_{n,E,k_{||}}$ for the incident state of the nth tunneling channel of the bulk Ge with energy E and $k_{||}$. The scattering-state wave function is obtained using the self-consistent Hamiltonian for the GA structures and that for the bulk Ge [15]. The tunneling eigenchannels are obtained by diagonalizing the transmission matrix, $t^\dagger t$ [27]. The physical meaning of $T(E)$ is the tunneling probability for a charge carrier energy E in one region of Ge to the tunnel passing through the oxide to the other region of Ge. As the number of channels increases linearly with A, $T(E)$ are proportional to A.

The lower panels of Figs. 2(b)–2(e) show the $T(E)/A$ for the GA structures with different oxide thicknesses. The red color corresponds to the DB IL, while the blue color corresponds to the HP IL. Note that $T(E)$ are zero in E inside the bulk Ge band gap because no propagating state

TABLE III. Calculated E_g^{ox}, VBO, CBO, W_{VBO}, and W_{CBO} by the LDA + U method for Ge(100)/a-GeO_2/Ge(100) structures.

Structure	GA1	GA2	GA3	GA4
E_g^{ox} (eV)	0.80	5.42	5.90	5.87
VBO (eV)	0.40	2.83	3.24	3.21
CBO (eV)	0.00	2.19	2.26	2.26
W_{VBO} (nm)	0.00	0.07	0.72	1.72
W_{CBO} (nm)	0.00	0.08	0.55	1.63

exists; $T(E)/A$ are zero from 0.0 to 0.4 eV in the Ge-based structures [Figs. 2(b)–2(e)]. If the DOX region is absent, no finite energy range with reduced $T(E)/A$ appears outside the band gap of Ge, similar to Fig. 2(b). In contrast, the presence of the DOX region, which acts as a potential barrier, greatly reduces the $T(E)/A$ in the energy range corresponding to the oxide band gap, as shown in Figs. 2(c)–2(e).

The decrement of $T(E)/A$ by the presence of oxide is typically different between holes and electrons. For the GA3 structure, the decrement of $T(E)/A$ at 1 eV below VBM^{Ge} and that at 1 eV above CBM^{Ge} are significantly different from each other, as indicated by the vertical black arrows in the lower panel of Fig. 2(d). This result is because the W_{VBO} (0.72 nm) is thicker than the W_{CBO} (0.55 nm), as indicated by the black arrows in the upper panel of Fig. 2(d), and because the VBO (3.24 eV) is larger than the CBO (2.26 eV). For simplicity, tunneling through a one-dimensional (1D) square potential barrier with height V_o and width $2a$ is considered. In the limiting case of a very high and wide barrier, the square of the transmission amplitude is $T(E)_{1D} \cong \exp[-4\sqrt{2m(V_o - E)}(a/\hbar)]$ for $E < V_o$, showing that $T(E)_{1D}$ decreases drastically as the width $2a$ increases and the energy range for the decreased $T(E)_{1D}$ becomes wider as the potential barrier V_o becomes higher. These behaviors are also true for the 3D cases. The value of $T(E)/A$ decreases as the width of the band offset increases and $T(E)/A$ decreases within the charge carrier energy range of $VBM^{Ge} - VBO < E < VBM^{Ge}$ or $CBM^{Ge} < E < CBM^{Ge} + CBO$. Thus, $T(E)/A$ are affected differently by the width and magnitude of the band offset; the former affects only the decrement of $T(E)/A$ at each energy E, while the latter influences the energy range of the decreased $T(E)/A$, as well as the decrement itself.

Regarding the effects of the widths of the band offsets in the GA structures, there are two important points to note. First, due to the gradual increase of the band offsets from the IL to the DOX, the width of the band offset in the valence band is thickest near VBM^{Ge}, while that in the conduction band is thickest near CBM^{Ge}. This result correspondingly causes the smallest $T(E)/A$ near VBM^{Ge} and CBM^{Ge}. Second, the thicker W_{VBO} than W_{CBO} as well as the larger VBO than CBO induces smaller $T(E)/A$ near VBM^{Ge} than near CBM^{Ge}, resulting in asymmetry in $T(E)/A$ near the band gap of Ge. This result indicates a lower tunneling current density for the holes than the electrons, as shown in Fig. 3. Meanwhile, the larger VBO than CBO results in a wider energy range of the decreased $T(E)/A$ in the valence band than in the conduction band.

As d_{DOX} increases up to the approximate critical thickness of approximately 1 nm in the GA structures, the $T(E)/A$ values near VBM^{Ge} and CBM^{Ge} drastically decrease due to the increase of W_{VBO} and W_{CBO}, as well as the increase of VBO and CBO. The energy range of decreasing $T(E)/A$ becomes wider due to the increase of VBO and CBO with the increase of d_{DOX}. Meanwhile, as

TABLE IV. Structure information used for the transport calculations of Ge(100)/a-GeO_2/Ge(100) structures and theoretically estimated direct tunneling current densities, J_{DT} (A cm^{-2}), calculated in an infinite boundary condition along the z axis by the LDA + U method. The information for J_e, J_h:DB IL, HP IL:n_e, or n_h values (cm^{-3}) is given.

Structure	GA1	GA2	GA3	GA4
Length along z (nm)	3.619	4.069	4.468	5.398
Number of Ge/O	191/18	204/40	216/64	248/128
J_e:DB:10^{18}	2.0×10^6	1.3×10^4	6.5×10^2	5.9×10^{-1}
J_e:DB:10^{20}	5.7×10^7	1.7×10^6	2.1×10^4	6.3×10^1
J_e:HP:10^{18}	1.9×10^6	2.4×10^4	8.2×10^2	1.4×10^0
J_e:HP:10^{20}	5.7×10^7	1.8×10^6	2.5×10^4	7.3×10^1
J_h:DB:10^{18}	2.1×10^4	1.3×10^3	4.1×10^1	1.0×10^0
J_h:DB:10^{20}	2.8×10^6	5.2×10^4	2.0×10^3	2.2×10^2
J_h:HP:10^{18}	2.1×10^4	2.4×10^3	1.8×10^1	2.2×10^{-1}
J_h:HP:10^{20}	2.8×10^6	1.6×10^5	2.2×10^3	1.7×10^1

d_{DOX} increases above the approximate critical thickness of approximately 1 nm, only the magnitude of $T(E)/A$ within the fully formed E_g^{ox} rapidly decreases such as from the GA3 structure [Fig. 2(d)] to the GA4 structure [Fig. 2(e)] because the GA3 structure has almost full VBO and CBO, as mentioned earlier. Therefore, in sub-1-nm-thick oxide, the increase of the oxide thickness induces the decrease of the $T(E)/A$ in the wider energy range, suppressing the $T(E)/A$ more strongly inside E_g^{ox}.

Next, the effect of the two different interfacial structures of the DB IL and HP IL on the tunneling properties is discussed. As shown in Figs. 2(b)–2(e), the $T(E)/A$ values for the DB IL and the HP IL are very similar. This fact is confirmed in most of the GA structures including structures in Table V. This indicates that the H passivation has a minor effect on the $T(E)/A$ at the interface between the semiconductor and the amorphous oxide. For example, as shown in Fig. 2(d), the H passivation hardly reduces the peak near $\mathrm{CBM}^{\mathrm{Ge}}$ in the $T(E)/A$ for the GA3 structure induced from the interface states. This ineffectiveness is presumably due to the irregular bonds at the interface between Ge and amorphous oxide, which is represented by the discrepancy in the number of defects and in the number of H atoms shown in Table II. Exceptionally, the peaks near $\mathrm{VBM}^{\mathrm{Ge}}$ in the $T(E)/A$ for the GA4 structure are significantly reduced due to the effective passivation by the H atoms. This result is relevant to the fact that the number of defects and the number of H atoms are identical only in the GA4 structure, as shown in Table II. On the contrary, in the previous study [7], the H passivation of the dangling bonds in the Si/c-SiO_2/Si structures greatly reduced the $T(E)/A$, especially near $\mathrm{VBM}^{\mathrm{Si}}$, implying the effectiveness of H passivation at the interface between the semiconductor and the crystalline oxide.

Using $T(E)/A$, the direct tunneling current density per unit area, J_{DT}, is estimated as a function of the electron (n_e) and hole concentrations (n_h). The electron tunneling current density, J_e, in the conduction bands can be calculated using the equation $J_e = 2e/Ah\int_{\mathrm{CBM}}^{\infty} T(E)f\,(E)dE$, and the hole tunneling current density, J_h, in the valence bands can be estimated using the equation $J_h = 2e/Ah\int_{-\infty}^{\mathrm{VBM}} T(E)[1-f\,(E)]dE$. Here, $f(E)$ is the Fermi-Dirac distribution function at 300 K in the Ge region, h is the Planck constant, and A is the cross-sectional area. Although the more precise calculation of J_e and J_h requires taking into account the current flux in the opposite direction, the current flux in the opposite direction [$J_e = -2e/Ah\int_{\mathrm{CBM}}^{\infty} T(E)f\,(E+V)dE$] is negligible for the usual bias voltage (V) range of kT $\ll V \ll$ barrier height at the semiconductor/insulator junction. Moreover, $T(E)$ also have a V dependency due to the modification of the barrier profile under the application of V. This aspect is also disregarded because, under the condition of $V \ll$ barrier height (direct tunneling regime), its influence is also not significant. Nonetheless, these calculation results can be taken as the appropriate minimum tunneling leakage current when a small V is applied to the semiconductor/oxide junction system. The calculated J_{DT} corresponds to the gate leakage current density when V is small enough so that change in $T(E)/A$ is negligible.

It is assumed that n_e or n_h is close to the substrate doping concentration because J_e and J_h are associated with the tunneling from the channel to the gate. In fact, this calculation can be applied quite efficiently to various cases in MOS field effect transistor (MOSFET) operation and device performance evaluation. When the device is under normal operation, i.e., the semiconductor changes from inversion [the region shown in Fig. 3(a)]

TABLE V. Relaxed atomic structures of Ge(100)/a-GeO_2/Ge(100), Ge(110)/a-GeO_2/Ge(110), and Ge(111)/a-GeO_2/Ge(111) structures with similar oxide thicknesses. The 100_2 structure is the same as the GA3 structure in Table II.

Ge orientation		(100)			(110)			(111)	
Structure	100_1	100_2	100_3	110_1	110_2	110_3	111_1	111_2	111_3
Supercell along z (nm)	5.535	5.597	5.569	6.638	6.646	6.708	4.636	4.774	5.466
Number of Ge/O	288/64	288/64	288/64	368/64	368/64	368/64	208/64	208/64	240/64
A (nm^2)		1.129×1.129			1.129×1.197			0.798×1.382	
d_{TOX} (nm)	1.318	1.354	1.475	1.377	1.370	1.422	1.436	1.585	1.863
d_{DOX} (nm)	0.774	0.854	0.927	0.839	0.842	0.930	0.928	1.027	1.007
$d_{\mathrm{DOX,ave}}$ (nm)		0.852			0.870			0.987	
d_{IL} (nm)	0.272	0.250	0.274	0.269	0.264	0.246	0.254	0.279	0.428
$d_{\mathrm{IL,ave}}$ (nm)		0.265 ± 0.024			0.259 ± 0.026			0.320 ± 0.130	
Numbers of suboxide states, defects, and H atoms in the ILs									
Ge^{1+}	4	10	8	9	8	11	3	13	7
Ge^{2+}	8	4	5	1	3	2	3	0	4
Ge^{3+}	3	5	5	5	7	5	4	3	3
Ge^{4+}	1	1	0	1	1	0	1	0	1
Defect (DB)	8	7	5	8	8	6	4	6	7
H (HP)	8	2	5	4	8	3	4	1	7

to accumulation-depletion [the off-subthreshold region shown in Fig. 3(b)] and vice versa, by the positive gate bias in the n-type MOSFET (nMOS), the electron injection from the inverted channel to the gate matters. If this injection is too high, the active power consumption becomes uncontrollable even if the drain current is higher than the gate leakage current. In modern nMOS devices, the channel doping is approximately 10^{18} cm^{-3} so that the electron density of the inversion region is of the same order of magnitude, meaning that n_e can be taken as 10^{18} cm^{-3} for this active leakage current calculation. In this case, the gate voltage is shared by the gate insulator and channel and, with the small threshold voltage ($V_{\text{th}} <\sim 0.5$ V) of nMOS, the voltage drop across the gate insulator is much smaller than the electron barrier height, satisfying the above assumption ($V \ll$ barrier height).

In contrast, when the nMOS device is under the off state or under the test condition of dielectric reliability of the gate insulator, the gate bias has a negative sign. In this case, the band bending in the semiconductor channel becomes minimal (up to the local chemical potential, μ, mentioned below) and most of the voltage drop occurs in the gate insulator. Under this circumstance, the electron injection from the semiconductor channel to the gate is negligible because there are almost no electrons within the channel region. In contrast, the electron injection from the gate, where n_e is as high as 10^{20} cm^{-3}, becomes the dominant tunneling leakage current mechanism. Fortunately, J_e can be similarly calculated using the same formula, by simply taking $n_e = 10^{20}$ cm^{-3}, as long as the gate voltage $V \ll$ barrier height, which is mostly the case. There could be J_h from the channel to the gate, but this must be much smaller than the above-mentioned J_e due to the smaller n_h and the greater barrier height for the holes than the electrons. Therefore, the total leakage current is reasonably well represented by the electron injection from the gate to the channel. Again, the calculation results represent the lower leakage current boundary at a small bias voltage.

For the p-type MOSFET (pMOS), identical arguments can be applied using all the parameters for the hole-related ones. The gate bias has a negative polarity during the normal pMOS-on operation, and has a positive polarity during the pMOS-off operation and the reliability test.

The theoretical local chemical potentials, μ, for n_e and n_h for the GA structure are determined from the density of states of bulk Ge, such as $n_e = \int \text{DOS}_{\text{Ge}}(E) f(E) dE$ and $n_h = \int \text{DOS}_{\text{Ge}}(E)[1 - f(E)]dE$. They are located at 0.021 eV below CBM for $n_e = 10^{18}$ cm^{-3} (at 0.160 eV above CBM for $n_e = 10^{20}$ cm^{-3}) and at 0.038 eV above VBM for $n_h = 10^{18}$ cm^{-3} (at 0.127 eV below VBM for $n_h = 10^{20}$ cm^{-3}).

When VBO or CBO corresponds to the barrier height of the charge carriers, Φ_b, the direct tunneling current density, J_{DT}, is expressed by a semiempirical formula, as follows [28,29]:

$$J_{\text{DT}} \propto \frac{f(\Phi_b)}{\kappa \Phi_b} \exp\left[-\frac{2\sqrt{2|q|}}{\hbar} (m_{\text{eff}}\Phi_b)^{1/2} \kappa \text{ EOT}\right],$$

where q and m_{eff} are the charge and effective mass of the electrons or holes, respectively; $f(\Phi_b)$ is a function of the potential barrier (Φ_b); κ is the relative optical dielectric constant of the oxide; and EOT is the equivalent oxide thickness. For the sub-1-nm-thick oxide, Φ_b is not constant but varies depending on the DOX thickness.

Figures 3(c) are the calculated direct tunneling current density of the holes and electrons, J_h and J_e, in log scale, as a function of d_{DOX} for the GA structures in the case of $n_{e,h} = 10^{18}$ cm^{-3}, respectively. The red color indicates the DB IL and the blue color indicates the HP IL. The calculated J_{DT} decays almost exponentially with respect to d_{DOX}, which is in accordance with the fact that d_{DOX} is the effective thickness of the potential barrier for charge carriers, not d_{TOX}, due to the existence of the IL. Table IV shows J_e and J_h with respect to n_e, n_h, DB IL, and HP IL. In these results, J_e is always higher than J_h, which originates from the thicker W_{VBO} than W_{CBO} and the larger VBO than CBO. As discussed previously, a thicker W_{VBO} than W_{CBO} and a larger VBO than CBO induce a further decreasing

TABLE VI. Calculated E_g^{ox}, VBO, CBO, W_{VBO}, W_{CBO}, and their average values by the LDA + U method for Ge/a-GeO_2/Ge structures with different Ge orientations and similar oxide thicknesses.

Structure	100_1	100_2	100_3	110_1	110_2	110_3	111_1	111_2	111_3
E_g^{ox} (eV)	4.83	5.90	5.80	5.57	5.16	5.39	5.80	5.76	5.55
$E_{g,\text{ave}}^{\text{ox}}$ (eV)		5.51			5.37			5.70	
VBO (eV)	2.71	3.24	3.13	3.55	2.59	2.87	3.20	3.11	2.93
CBO (eV)	1.72	2.26	2.27	1.62	2.17	2.12	2.20	2.25	2.22
VBO_{ave} (eV)		3.03			3.00			3.08	
CBO_{ave} (eV)		2.08			1.97			2.22	
W_{VBO} (nm)	0.67	0.72	0.70	0.78	0.78	0.87	0.79	0.98	0.91
W_{CBO} (nm)	0.47	0.55	0.44	0.34	0.58	0.42	0.52	0.58	0.62
$W_{\text{VBO,ave}}$ (nm)		0.70			0.81			0.89	
$W_{\text{CBO,ave}}$ (nm)		0.49			0.45			0.57	

tendency of $T(E)/A$ in the valence bands than in the conduction bands, resulting in a lower J_h than J_e. In addition, the $T(E)/A$ values near $\mathrm{VBM^{Ge}}$ or $\mathrm{CBM^{Ge}}$ are most important because $T(E)/A$ are integrated dominantly near these energy ranges in order to estimate J_{DT}. The J_{DT} of the GA structure with the HP IL tends to be slightly lower than that with the DB IL, indicating that H passivation does not have a crucial effect on tunneling.

Figures 3(d) and 3(e) show the effects of the band-gap correction of Ge from 0.4 eV (red/blue) to 0.7 eV (black) on the $T(E)/A$ and the J_{DT}. The increase in the band gap of Ge from 0.4 to 0.7 eV results in the downshift of the VBO by 0.2 eV and upshift of the CBO by 0.1 eV for all the GA structures. Consequently, the band-gap increase causes the parallel shift of $T(E)/A$ by approximately -0.2 eV in the valence bands and by approximately 0.1 eV in the conduction bands, as shown in Fig. 3(d), keeping similar $T(E)/A$ values near the $\mathrm{VBM^{Ge}}$ and $\mathrm{CBM^{Ge}}$ due to small changes in the band offsets. On the other hand, the effects of the band gap increase from 0.4 (open blue/red) to 0.7 eV (closed black) on J_{DT} are not significant, as shown in Fig. 3(e), because of the similarly retained $T(E)/A$ values near the $\mathrm{VBM^{Ge}}$ and $\mathrm{CBM^{Ge}}$, which are important to estimate J_{DT}.

To examine the effect of the Ge orientation on the electronic structures and tunneling properties, Ge/a-GeO_2/Ge structures, where the Ge(100), (110), and (111) surfaces form interfaces with a-GeO_2, are generated, as shown in Fig. 4(a). For each Ge orientation, three different structures with similar d_{DOX} values are investigated, as shown in Table V. In accordance with the H passivation procedure in the manufacturing of Ge-based devices and the minor effect of H passivation on the tunneling currents at the interface between the semiconductor and the amorphous oxide, only the HP IL structures are considered. Figure 4(b) shows the d_{DOX}, d_{IL}, and d_{TOX} values, where the average values are indicated as a histogram, with the maximum and minimum values indicated as bars at the top of the histogram. In Tables II and V, the average d_{IL} is 0.282 ± 0.028 nm regardless of the Ge orientation for all the Ge/a-GeO_2/Ge structures, including the GA1–GA4 structures. In Table V, the range of the d_{DOX} values is 0.8–1.0 nm for all the structures, irrespective of the orientation, and the difference in d_{DOX} for each orientation is less than 0.1 nm. From the smaller difference in d_{DOX} among the orientations than the interlayer spacing of approximately 0.13, approximately 0.19, and approximately 0.24/0.08 nm in the bulk Ge(100), (110), and (111), respectively, the E_g^{ox}, VBO, CBO, W_{VBO}, and W_{CBO} are averaged over three different structures for each orientation, as summarized in Table VI.

Figure 4(c) shows the VBO, CBO, and the band gap in the a-GeO_2 region (E_g^{ox}). E_g^{ox} values ranges from 4.83–5.90 eV and their average value is 5.5 eV. The VBO is commonly larger than the CBO and Table VI shows that

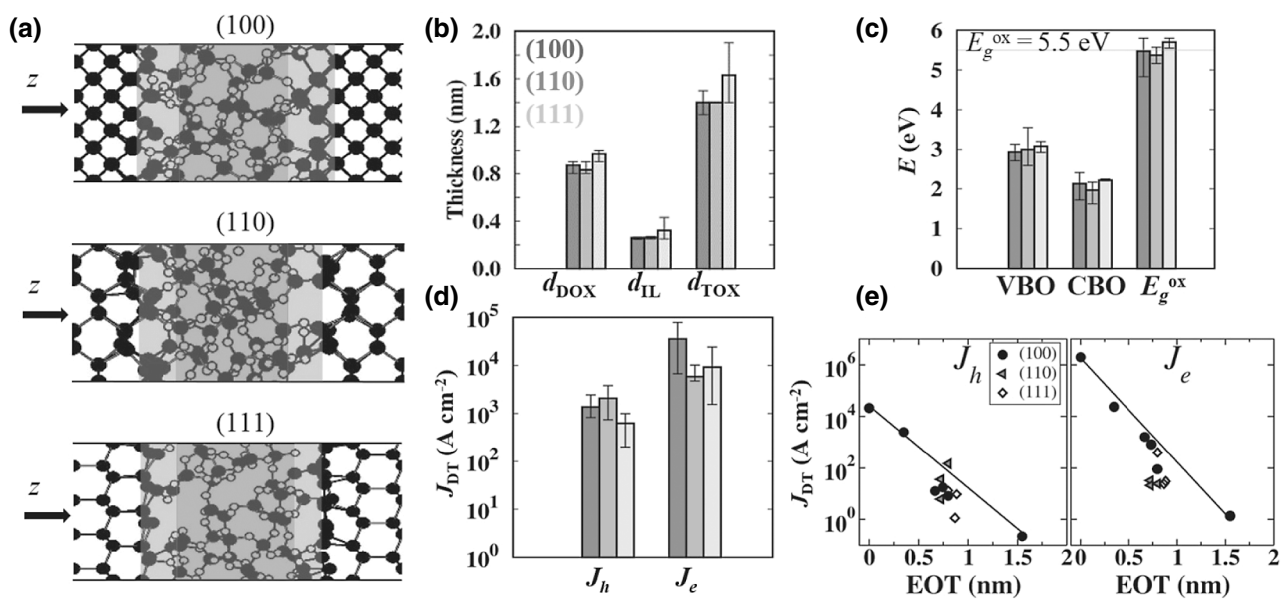

FIG. 4. (a) Relaxed atomic structures of Ge(100)/GeO_2/Ge(100), Ge(110)/GeO_2/Ge(110), and Ge(111)/GeO_2/Ge(111) with the DB IL. The IL and DOX are colored light and dark gray, respectively. (b) Average d_{DOX}, d_{IL}, and d_{TOX} in the histogram for each Ge orientation. The maximum and minimum values are shown by bars. (c) Average VBO, CBO, and band gap in the a-GeO_2 region (E_g^{ox}). (d) Average tunneling current densities for the hole (J_h) and the electron (J_e). The band offsets and J_{DT} in (c)–(e) are obtained from the structures with the HP IL and a 10^{18} cm^{-3} $n_{e,h}$ value is used for J_{DT}. (e) J_{DT} vs EOT for all the structures. The solid line is drawn from the minimum to the maximum J_{DT} for visual guidance.

TABLE VII. Structure information used for the transport calculations for Ge/a-GeO_2/Ge structures with different Ge orientations and similar oxide thicknesses and the theoretically estimated tunneling current densities, J_{DT} (A cm^{-2}), calculated in an infinite boundary condition along the z axis by the LDA + U method. The information for J_e, J_h:DB IL, HP IL:n_e, or n_h values (cm^{-3}) is given.

Structure	100_1	100_2	100_3	110_1	110_2	110_3	111_1	111_2	111_3
Length along z (nm)	4.407	4.468	4.441	5.241	5.250	5.311	3.903	4.041	4.733
Number of Ge/O	216/64	216/64	216/64	272/64	272/64	272/64	160/64	160/64	192/64
J_e:HP:10^{18}	1.6×10^3	8.2×10^2	8.9×10^1	3.2×10^1	2.1×10^1	2.4×10^1	4.0×10^2	3.0×10^1	2.4×10^1
J_e:HP:10^{20}	7.9×10^4	2.5×10^4	6.7×10^3	1.0×10^4	2.6×10^3	4.8×10^3	2.4×10^4	1.9×10^3	1.5×10^3
J_h:HP:10^{18}	1.3×10^1	1.8×10^1	8.3×10^0	6.1×10^0	3.6×10^1	1.5×10^2	1.3×10^1	9.6×10^0	1.1×10^0
J_h:HP:10^{20}	8.3×10^2	2.2×10^3	8.3×10^2	7.4×10^2	1.7×10^3	3.8×10^3	9.9×10^2	6.8×10^2	2.0×10^2

W_{VBO} is also commonly thicker than W_{CBO}, with no obvious dependencies of VBO, CBO, W_{VBO}, and W_{CBO} on the Ge orientation. This result may be attributed to the fact that the interfacial structure is not significantly different among the different orientations due to the disordered atomic structure of amorphous oxide. As a result, J_e is commonly higher than J_h, as shown in Fig. 4(d), irrespective of the Ge orientation. The values of J_e and J_h for the different n_e and n_h, respectively, are listed in Table VII. Figure 4(e) shows the J_{DT} for all the Ge/a-GeO_2/Ge structures, including the four GA structures (GA1, GA2, GA3, GA4) in the case of $n_{e,h}$=10^{18} cm^{-3}, as a function of EOT, where the EOT is estimated to be $\kappa_{a\text{-}SiO_2}/\kappa_{a\text{-}GeO_2} \times d_{DOX,a\text{-}GeO_2} = 3.9/4.5 \times d_{DOX,a\text{-}GeO_2} \cong 0.87 \times d_{DOX,a\text{-}GeO_2}$ by using the experimental static dielectric constant κ of 4.5 for the bulk a-GeO_2 [30] and 3.9 for the bulk a-SiO_2 [31]. The current density J_e or J_h shows exponential decay as a function of EOT regardless of the Ge orientation, as can be seen in Fig. 4(e). Therefore, it is concluded that the Ge orientation has no significant effect on the electronic structure and the tunneling properties.

III. CONCLUSION

The correlations among the atomic structures, bandgap evolution, and tunneling spectra in the sub-2-nm-thick oxides in Ge/a-GeO_2/Ge structures with respect to the oxide thicknesses, interfacial structures, and Ge orientations are presented. The thickness of the stoichiometric dioxide region excluding the interface layer (IL) is suggested as the effective tunneling-blocking oxide thickness and it is applicable to other semiconductor/native oxide structures. The proposed critical oxide thickness for the thinnest usable a-GeO_2 is approximately 0.85 nm. It is found that the smaller tunneling current density of the holes than of the electrons results from the larger magnitude and thicker widths of the VBO than those of the CBO, which is also valid in other semiconductor insulator/semiconductor structures with a larger VBO than CBO. The hydrogen passivation at the semiconductor/a-oxide interface is not effective in reducing the tunneling current. The crystallographic orientation of the Ge substrate is found to have no obvious effect on the tunneling current in semiconductor/a-oxide/semiconductor structures.

ACKNOWLEDGMENTS

The authors acknowledge the support provided by the Future Semiconductor Device Technology Development Program (Grant No. 10048490) funded by MOTIE and KSRC, and by the Institutional Research Program of KIST (Grant No. 2E29390). E.K. also acknowledges the Program for Returners into R&D (WISET Grants No. 2016-251, No. 2017-337, and No. 2018-310) of NRF and WISET funded by MSIT, Korea. The authors would also like to acknowledge the support from KISTI Supercomputing Center through the Strategic Support Program for Supercomputing Application Research (Grants No. KSC-2016-C3-0023 and No. KSC-2017-C3-0035). E.K. performed and analyzed all the calculations. K.L. assisted in the generation of the atomic structures and discussed the technical contexts. C.S.H. helped in the preparation of the manuscript from the viewpoint of an expert in nanoelectronic devices. H.J.C. provided the transport code and discussed the technical issues. J.-H.C. arranged, supervised all the calculations, and took charge of the manuscript preparation. All the authors discussed and reviewed the manuscript.

APPENDIX: COMPUTATIONAL METHODS

The atomic and electronic structures are calculated using the first-principles density-functional method as implemented in the Siesta code [32] and the tunneling spectra are computed using the first-principles scattering-state method as implemented in the Scarlet code [15]. The norm-conserving pseudopotentials [33] are used for the electron-ion interactions. Real-space grids are generated with 200-Ry cutoff energy and pseudoatomic orbitals (triple ζ polarization for Ge or Si and double ζ polarization for O) are used to expand the electronic wave functions. For the Brillouin-zone integration, a $4 \times 4 \times 1$ k-grid for the structure relaxation, a $12 \times 12 \times 1$ k-grid for the electronic structure, and an 8×8 $k_{||}$-grid for the tunneling spectra are used, respectively.

To construct heterostructures of GA structures, an oxide slab is placed between two Ge(100) slabs, with an approximately 0.1-nm initial separation distance between the Ge and a-GeO_2. The in-plane dimension is a $2a_{Ge} \times 2a_{Ge}$ supercell, as presented in Table II. Other orientations are also created by placing an amorphous oxide slab between two Ge(110) or Ge(111) slabs; thus, they have different in-plane supercell sizes from those with the Ge(100) orientation, as shown in Table V. The generation procedures of heterostructures are concretely explained in the Supplemental Material [16].

Preliminary calculations are performed to obtain the lowest energy Ge/a-GeO_2/Ge structure from the initially same Ge and a-GeO_2 slabs using different relaxation conditions. The total energy and numbers of defects at the IL and the d_{IL} are compared and their tunneling properties are also extensively explained in the Supplemental Material [16]. From these preliminary calculations, the lowest energy structure is obtained by relaxing the supercell size along the z axis, as well as relaxing the atoms inside the amorphous oxide and Ge layers near the interface. The lowest energy structure has the minimum number of defects at the IL and the thinnest d_{IL}. Therefore, all the structures in Tables II and V are generated through this relaxation scheme until all the atomic forces are smaller than 0.05 eV/Å.

[1] P. S. Goley, and M. K. Hudait, Germanium based field-effect transistors: Challenges and opportunities, J. Mater. Sci. **7**, 2301 (2014).

[2] C. O. Chui, S. Ramanathan, B. B. Triplett, P. C. McIntyre, and K. C. Saraswat, Germanium MOS capacitors incorporating ultrathin high-k gate dielectric, IEEE Electron Device Lett. **23**, 473 (2002).

[3] C. O. Chui, F. Ito, and K. C. Saraswat, Scalability and electrical properties of germanium oxynitride MOS dielectrics, IEEE Electron Device Lett. **5**, 613 (2004).

[4] R. Zhang, T. Iwasaki, N. Taoka, M. Takenaka, and S. Takagi, High-mobility Ge pMOSFET with 1-nm EOT Al_2O_3/GeO_x/Ge gate stack fabiricated by plasma post oxidation, IEEE Trans. Electron Devices **59**, 335 (2012).

[5] A. A. Demkov, X. Zhang, and D. A. Drabold, Towards a first-principles simulation and current-voltage characteristic of atomistic metal-oxide-semiconductor structures, Phys. Rev. B **64**, 125306 (2001).

[6] J. Kang, Y.-H. Kim, J. Bang, and K. J. Chang, Direct and defect-assisted electron tunneling through ultrathin SiO_2 layers from first principles, Phys. Rev. B **77**, 195321 (2008).

[7] E. Ko, K.-R. Lee, and H. J. Choi, Effects of interfacial suboxides and dangling bonds on tunneling current through nanometer-thick SiO_2 layers, Phys. Rev. B **84**, 033303 (2011).

[8] E. Ko, K.-R. Lee, and H. J. Choi, Tunneling properties versus electronic structures in $Si/SiO_2/Si$ junctions from first-principles, Phys. Rev. B **88**, 035318 (2013).

[9] S. Shibayama, T. Yoshida, K. Kato, M. Sakashita, W. Takeuchi, N. Taoka, O. Nakatsuka, and S. Zaima, Formation of chemically stable GeO_2 on the Ge surface with pulsed metal-organic chemical vapor deposition, Appl. Phys. Lett. **106**, 062107 (2015).

[10] J. F. Binder, P. Broqvist, H.-P. Komsa, and A. Pasquarello, Germanium core-level shifts at Ge/GeO_2 interfaces through hybrid functionals, Phys. Rev. B **85**, 245305 (2012).

[11] H. Matsubara, T. Sasada, M. Takenaka, and S. Takagi, Evidence of low interface trap density in GeO_2/Ge metal-oxide-semiconductor structures fabricated by thermal oxidation, Appl. Phys. Lett. **93**, 032104 (2008).

[12] A. Delabie, F. Bellenger, M. Houssa, T. Conard, S. V. Elshocht, M. Caymax, M. Heyns, and M. Meuris, Effective electrical passivation of Ge(100) for high-k gate dielectric layers using germanium oxide, Appl. Phys. Lett. **91**, 082904 (2007).

[13] T. Low, M.-F. Li, G. Samudra, Y.-C. Yeo, C. Zhu, A. Chin, and D.-L. Kwong, Modeling study of the impact of surface roughness on silicon and germanium UTB MOSFETs, IEEE Trans. Electron Devices **52**, 2430 (2005).

[14] T. Sasada, Y. Nakakita, M. Takenaka, and S. Takagi, Surface orientation dependence of interface properties of GeO_2/Ge metal-oxide-semiconductor structures fabricated by thermal oxidation, J. Appl. Phys. **106**, 073716 (2009).

[15] H. J. Choi, M. L. Cohen, and S. G. Louie, First-principles scattering-state approach for nonlinear electrical transport in nanostructures, Phys. Rev. B **76**, 155420 (2007).

[16] See Supplemental Material at http://link.aps.org/supplemental/10.1103/PhysRevApplied.11.034016 for details on preparation of Ge/a-GeO_2/Ge heterostructures and discussion of the model-dependent changes in tunneling properties.

[17] J. Lee, Y. Kang, S. Han, C. S. Hwang, and J.-H. Choi, Ab initio study on the structural characteristics of amorphous Zn_2SnO_4, Appl. Phys. Lett. **103**, 252102 (2013).

[18] J. Park, J. Lee, C. S. Hwang, and J.-H. Choi, Atomic and electronic structures of a-$ZnSnO_3$/a-SiO_2 interface by *ab initio* molecular dynamics simulations, Phys. Status Solidi B **253**, 1765 (2016).

[19] R. Weast, *CRC Handbook of Chemistry and Physics* (CRC Press, Cleveland, 1997), 78th ed.

[20] N. M. Ravindra, R. A. Weeks, and D. L. Kinser, Optical properties of GeO_2, Phys. Rev. B **36**, 6132 (1987).

[21] V. Anisimov, J. Zaanen, and O. Andersen, Band theory and mott insulators: Hubbard U instead of stoner I, Phys. Rev. B **44**, 943 (1991).

[22] M. Cococcioni, and S. deGironcoli, Linear response approach to the calculation of the effective interaction parameters in the LDA + U method, Phys. Rev. B **71**, 035105 (2005).

[23] J. C. Ranuárez, M. J. Deen, and C.-H. Chen, A review of gate tunneling current in MOS devices, Microelectron. Relia. **46**, 1939 (2006).

[24] F. Giustino, and A. Pasquarello, Electronic and dielectric properties of a suboxide interlayer at the silicon-oxide interface in MOS devices, Surf. Sci. **586**, 183 (2005).

[25] W. F. Zhang, T. Nshimula, K. Nagashio, K. Kita, and A. Toriumi, Conduction band offset at GeO_2/Ge interface determined by internal photoemission and charge-corrected

x-ray photoelectron spectroscopies, Appl. Phys. Lett. **102**, 102106 (2013).

[26] D. A. Muller, T. Sorsch, S. Moccio, F. H. Baumann, K. EvansLutterodt, and G. Timp, The electronic structure at the atomic scale of ultrathin gate oxides, Nature **399**, 758 (1999).

[27] M. Brandvyge, M. R. Sorensen, and K. W. Jacobsen, Conductance eigenchannels in nanocontacts, Phys. Rev. B **56**, 14956 (1997).

[28] E. M. Vogel, K. Z. Ahmed, B. Hornung, W. K. Henson, and P. K. McLarty, Modeled tunnel currents for high dielectric constant dielectrics, IEEE Trans. Electron Devices **45**, 1350 (1998).

[29] Y.-C. Yeo, T.-J. King, and C. Hu, MOSFET gate leakage modeling and selection guide for alternative gate dielectrics based on leakage considerations, IEEE Trans. Electron Devices, **50**, 1027 (2003).

[30] S. N. A. Murad, P. T. Baine, D. W. McNeill, S. J. N. Mitchell, B. M. Armstrong, M. Modreanu, G. Hughes, and R. K. Chellappan, Optimisation and scaling of interfacial GeO_2 layers for high-*k* gate stacks on germanium and extraction of dielectric constant of GeO_2, Solid-State Electron. **78**, 136 (2012).

[31] S. Sze, *Physics of Semiconductor Devices* (John Wiley and Sons, New York, 1981).

[32] D. Sánchez-Portal, P. Ordejón, E. Artacho, and J. M. Soler, Density-functional method for very large systems with LCAO basis sets, Int. J. Quantum Chem. **65**, 453 (1997).

[33] N. Troullier, and J. L. Martins, Efficient pseudopotentials for plane-wave calculations, Phys. Rev. B **43**, 1993 (1991).